Available online at www.sciencedirect.com
SCIENCE DIRECT®
International Journal of Thermal Sciences 44 (2005) 756–765
International Journal of Thermal Sciences
www.elsevier.com/locate/ijts

Undeveloped convective heat transfer from an array of cubes in cross-stream direction

Mahmood Yaghoubi [a,*], Ehsan Velayati [b]

[a] *Mechanical Engineering Department, School of Engineering, Shiraz University, Shiraz 71345, Iran*
[b] *Saady St., Mohammad-Javad Mostafaee alley, No. 17, Najaf-Abad 85137, Iran*

Received 29 August 2003; received in revised form 3 February 2005; accepted 9 February 2005

Available online 23 March 2005

Abstract

Conjugate heat transfer for three-dimensional developing turbulent flows over an array of cubes in cross-stream direction, representing finite heat elements mounted over a surface is studied numerically. Incompressible fluid flow over the cubes is modeled using a fully elliptic form of the Navier–Stokes equations. RNG based k–ε turbulent model is incorporated to predict turbulent flow field as well as the recirculating pattern along the blocks. Temperature fields in the blocks and on their outer surfaces were obtained solving heat conduction equation. Finite volume procedure with appropriate boundary conditions is used to solve the coupling between the solid and fluid region. The heat transfer characteristics resulting from recirculating zone around the blocks are presented for a wide range of Reynolds numbers from 4.2×10^3 to 1×10^5 (for $Pr = 0.7$) and blockage ratios from 10 to 50%. Numerical computation is validated with experimental studies of Nakamura et al. [Internat. J. Heat Mass Transfer 44 (2001) 3385] and variation of the Nusselt number as well as fin efficiency in terms of flow Reynolds number and blockage ratios are determined. New correlations is developed to predict average Nusselt number as $\overline{Nu} = 0.11Re^{0.702}(1 + 0.68Br)$. Also a new correlation is obtained for fin efficiency such as $\eta_f = 126.69Re^{-0.027}(1 + Br)^{-0.035}$ for an array of inline cubes. The analysis is extended to study the effects of spacing between heat sources for a fixed heat input.

Keywords: Cubes; Conjugate heat transfer; Separation; Cross-stream mixing; Nusselt number; Fin efficiency

1. Introduction

The theory of forced convection in recirculating flows has gained a wide popularity in the subject of enhanced heat transfer. To improve heat transfer coefficient, the first step is to use extended surfaces. Such surface extension increases the total area of heat transfer and if it is installed correctly, the efficiency of the heat exchange surfaces will be improved. The efficiency will be further increased when the growing boundary layers are disrupted or when a cross-stream mixing is promoted. Usually this is made by introducing fins or cubes into the flow and arranging them in the channel to cause local changes in the mean flow direction and magnitude. A schematic of this kind of heat removal elements is presented in Fig. 1.

For blocks attached over a base surface, such as ribbed surfaces, the flow over each block is no more two-dimensional and convective heat transfer is strongly depends on the geometric arrangement and upcoming flow properties. A schematic representation of the flow features (Hussein and Martinuzzi [2]) is shown in Fig. 2. Such complicated flow pattern strongly relates on the fluid Reynolds number and turbulent intensity as well as on the domain structure.

Flows over an isolated, wall-mounted cube have been subject of several past investigations. Casotr and Robins [1] performed some experiments with hot wire around a single mounted cube in a boundary layer wind tunnel with large channel to cube height ratio. They changed the Reynolds number from 3×10^4 and greater than 10^5 based on the cube height. Casotr and Robins [1] have concluded that the

* Corresponding author. Tel.: +98 711 2301672; fax: +98 711 6272060.
E-mail addresses: yaghoub@shirazu.ac.ir (M. Yaghoubi), e_velayati@yahoo.com (E. Velayati).

1290-0729/$ – see front matter
doi:10.1016/j.ijthermalsci.2005.02.003

Nomenclature

A_c	fin cross section area
A_f	fin area
Br	blockage ratio, (D/W)
c_μ, c_1, c_2	coefficients in turbulence model, 0.085, 1.42, 1.68
C_D	drag coefficient
C_f	friction factor coefficient
C_p	specific heat
D, W	blocks thickness and spacing
G	shear generation, $\mu_t(u_{i,j}+u_{j,i})u_{i,j}$
h	convection heat transfer coefficient
K	thermal conductivity of solid
k	turbulent kinetic energy, $\overline{u_i'u_i'}/2$
Nu, Nu_L	Nusselt number, $(hD)/\lambda$, $(hL)/\lambda$
p	pressure
P	fin parameter
Pr	Prandtl number
Re	Reynolds number, $(U_\infty D)/\nu$
S_{ij}	mean strain rate tensor, $(u_{i,j}+u_{j,i})/2$
S	$\sqrt{2S_{ij}S_{ij}}=\sqrt{G/\mu_t}$
T	temperature
T_b, T_s	base and surface temperature of fin
u_i	index notation of velocity components
$\overline{u_i', u_i'}$	turbulent Reynolds stress tensor
$\overline{u_i'T'}$	turbulent heat flux
x, y, z	directions of rectangular coordinate

Greek symbols

α	fluid thermal diffusivity
β	parameter in RNG k–ε model, 0.012
δ_{ij}	Kronecker delta function
ε	turbulent dissipation rate, $\mu(\overline{u_{i,j}'u_{i,j}'})/\rho$
η, η_0	parameters in RNG k–ε model, Sk/ε, 4.38
η_f	fin efficiency
λ, λ_t	total and turbulent thermal conductivity of fluid, $(\lambda_0+\lambda_t)$, $(C_p\mu_t/\sigma_t)$
λ_0	laminar thermal conductivity of fluid
μ, μ_t	total and eddy viscosity, $(\mu_0+\mu_t)$, $(c_\mu\rho k^2/\varepsilon)$
μ_0	laminar viscosity
ν	fluid kinematic viscosity
ρ	fluid density
σ_t	turbulent Prandtl number
$\sigma_k, \sigma_\varepsilon$	turbulent Prandtl numbers for diffusion of k and ε
τ_w	wall shear stress

Notes

∞	uniform free stream condition
i	$i=1,2,3$ Cartesian coordinate
i, j, k	tensor notation
in	variables imposed for the inlet boundary
j	derivative with respect to j direction
$\overline{}$	time average component of turbulent parameter
$'$	fluctuating component of turbulent parameter

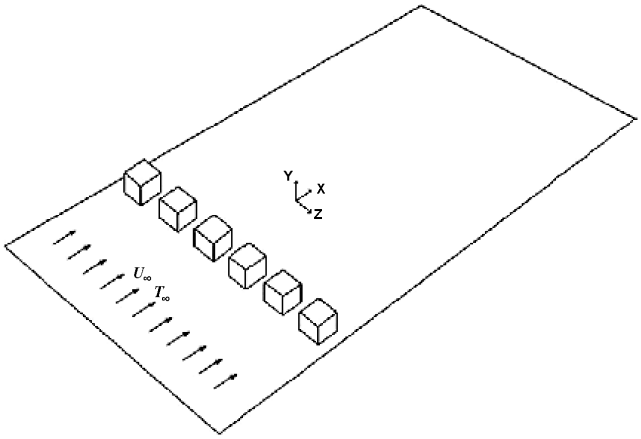

Fig. 1. The geometry of an array of cubes mounted over a surface ($Br=50\%$).

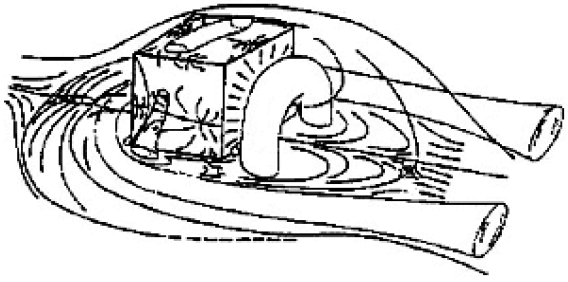

Fig. 2. Typical flow structure around a cube, Hussein and Martinuzzi [2].

shear and turbulence in the upstream flow provide a powerful mechanism for the rapid breakdown of the vortex system generated at the cube body. Regarding vortex shedding and periodically of the flow, they have noted that vortex shedding, if it occurs at all, will not be dominated and, more significant, the scale of turbulence in the upstream flow may not be very critical. However, cavity region is markedly reduced by the presence of upstream turbulence and from practical point of view, any vortex shedding for the case of a block with normal orientation to the flow can be ignored. Hussein and Martinuzzi [2] investigated experimentally the flow field around a surface mounted cube located in a wind tunnel with a fully developed turbulent flow condition. The height ratio of tunnel to cube was taken 2 which is quite small in comparison to the measurements of [1] and it is expected to have some different influences on the flow development. The Reynolds number based on the cube height is taken 40 000. Their results provide a detail insight to the evolution of the turbulence dissipation rate from the near field recirculation zone to the asymptotic wake. They have also performed oil

flow visualization and they found that the mean flow does not reattach on the top side and the wake recirculation region does not form a closed bubble. Hussein and Martinuzzi [2] also observed a saddle point on the channel floor adjacent to the trailing edge corner and along the reattachment line. Such flow condition produced a weak vortex shedding from the lateral surfaces with a constant frequency. The saddling flow behavior is different from the observations of Castro and Robins [1]. This may be attributed from different channel height ratio, turbulent intensity and or incoming boundary layer flow characteristics. Faghri and Asako [4] incorporated the Lam–Bremhorst low Reynolds number form of the k–ε turbulence model for periodic fully developed flow over modules having constant wall temperature. The assumption of spatially periodic flow boundary conditions [4, 5] only holds when there are fully developed condition and considerable blocks in both stream wise and cross stream wise direction. While the number of rows are few or there is a single row of blocks [6,7] or there is only an isolated block [1–3,8], the dynamic of fluid flow and vortical structure changes considerably and the results of flow and heat convection and conduction within the cubes will be strongly position dependent.

For a single array of wall-mounted cubical protrusions along a channel, Meinders et al. [7] recently performed a series of experiments to measure local convective heat transfer using infrared and liquid crystal thermography as well as oil-film visualization. It is found that for low Reynolds numbers range 795 to 6656, fluid flow and heat transfer is highly depends on the block position in the row. Meinders and Hanjalic [5] also investigated experimentally heat transfer from a matrix of equidistant cubes mounted on one of the walls of a plane channel. Also Meinders et al. [6] presented an experimental investigation of the application of an image restoration technique aimed to improve the accuracy of infrared surface temperature measurements of cubes placed in a vertical channel flow. Nakamura et al. [8] extended experimental investigation for fluid flow and heat transfer around a cube mounted on a wall of a plane in the turbulent boundary layer for Reynolds numbers of the range 4.2×10^3 to 3.3×10^4. They developed an empirical correlation for average overall Nusselt number around the cube as $\overline{Nu} = 0.138Re^{2/3}$, where Reynolds number is based on the height of the blocks. More recent studies for turbulent flow and heat transfer for a matrix of blocks belongs to Niceno et al. [9]. They have studied fluid flow and heat transfer from an internally heated multi-layered matrix of cubes mounted on a surface of a channel with low Reynolds number of 3854 based on the cube height. Present authors [10] reported numerical studies to predict turbulent flow and heat transfer around a single cube exposed to a cold stream. A correlation such as $\overline{Nu} = 0.112Re^{0.7}$ is developed to predict average convective heat transfer coefficient from a single block for the range of $4.2 \times 10^3 < Re < 4 \times 10^4$. Also the only related numerical studies concerning non-cubical obstacles belong to Velayati and Yaghoubi [11]. The blocks assumed to have aspect ratio 5 and Reynolds number changed from 5×10^3 to 3×10^4.

From the above review dealing with three-dimensional blocks [1–11], there is a not specific numerical study for turbulent flow around a single array of inline cubes in cross-stream direction, where the distance of the subsequent array may be very large. Also, no study is found from the present literature considering these three-dimensional cubes as heat removal fins or local surface roughness to increase heat transfer from the base plate. Moreover, practical correlation to predict heat transfer and fin efficiency is very limited for blocks which are attached to a base plate with wide space between them. In the present study, such cases will be analyzed, neglecting any saddling by assuming steady state condition as observed for large atmospheric boundary layer type flow by Castro and Robins [1]. Comparison of the results will be presented with available relations to validate the computed flow and heat transfer rate.

2. Governing equations

The governing equations for the three-dimensional steady state incompressible turbulent fluid flow are as follows:

2.1. Time-averaged equations

By applying time-averaging procedures to conservation equations, the equations that govern the mean-flow quantities, u_i, p and T, for turbulent flow are:

$$u_{j,j} = 0 \tag{1a}$$

$$\rho(u_j u_{i,j}) = -p_{,i} + \left[\mu(u_{i,j} + u_{j,i}) - \rho\overline{u_i' u_j'}\right]_{,j} \tag{1b}$$

$$\rho c_p(u_j T_{,j}) = \left(\lambda T_{,j} - \rho c_p \overline{u_j' T'}\right)_{,j} \tag{1c}$$

Applying the Boussinesq approximation, the Reynolds stress tensor and turbulent heat fluxes are:

$$-\rho\overline{u_i' u_j'} = 2\mu_t S_{ij} - \frac{2}{3}\rho k\delta_{ij} \tag{2a}$$

$$-\rho c_p \overline{u_i' T'} = \lambda_t T_{,i} \tag{2b}$$

2.2. RNG based k–ε turbulent model

In k–ε models, the turbulence field is characterized in terms of turbulent kinetic energy (k) and viscous dissipation rate of turbulent kinetic energy (ε). Yakhot et al. [12] proposed a variant of the k–ε model such that its performance characteristics were improved relative to the standard model. The RNG turbulence model is more responsive to the effects of rapid strain and streamlines curvature, flow separation, reattachment and recirculation than the standard k–ε model. The forms of the k and ε equations of the RNG model without buoyancy effects are as follows:

$$\rho u_j k_{,j} = \left(\left(\mu + \frac{\mu_t}{\sigma_k}\right)k_{,j}\right)_{,j} + G - \rho\varepsilon \tag{3a}$$

$$\rho u_j \varepsilon_{,j} = \left(\left(\mu + \frac{\mu_t}{\sigma_\varepsilon}\right)\varepsilon_{,j}\right)_{,j} + c_1 \frac{\varepsilon}{k} G - \frac{c_\mu \eta^3 (1-\eta/\eta_\circ)}{1+\beta\eta^3}\frac{\varepsilon^2}{k} - c_2 \rho \frac{\varepsilon^2}{k} \quad (3b)$$

The primary coefficients of the RNG model are provided by Yakhot et al. [12]. The terms $c_1 G(\varepsilon/k)$ and $c_2\rho(\varepsilon^2/k)$ in (3b) represent, respectively, the shear generation and viscous dissipation of ε. The extra term in (3b) employs the parameter η, which represents the ratio of characteristic time scales of turbulence and the mean flow fields, defined by $\eta = Sk/\varepsilon$. It can be shown that η is a function of the ratio of generation to dissipation of k and can be written as:

$$\eta = \sqrt{c_\mu^{-1}(G/\rho\varepsilon)} \quad (3c)$$

The temperature field in the block's mantle and on its outer surfaces (providing the appropriate boundary condition for the convection heat transfer) was obtained by solving the conduction equation simultaneously with heat convection in the fluid. This coupling of the temperature field and computation of the instantaneous block surface temperature is done by including conduction heat flux from the solid to the interface of the nearby control volume of the fluid cell. For heat conduction in the blocks, Fourier's equation was employed as:

$$T_{,jj} = 0 \quad (4)$$

3. Boundary conditions

To carry numerical computations, several attempts were made to identity the appropriate domain around the blocks. For unsteady state conditions, which may happen at low Reynolds numbers or high Reynolds numbers with certain boundary condition as illustrated by [2] vortex shedding may occur and this will lead to unsymmetrical flow field or saddling flow in certain region of the flow. For capturing any unsteadiness, first, a complete block ($D/W = 10\%$, $Re = 1\times10^5$) considered and computations performed for the full domain grids. For the considered conditions a completely symmetric results was obtained and it was found a steady state regime as illustrated by [1]. The possibility of flow transient to unsteady conditions for the present Reynolds numbers and flow boundary conditions is absent. Based on this result and from the symmetry in the considered geometry, for the rest of studies, the computational domain can be an isolated half of the channel, containing the half section of a block as illustrated in Fig. 3. For plane ABba, at the inlet boundary, uniform flow conditions are imposed for all variables using $u_{\text{in}} = U_\infty$, $v_{\text{in}} = 0$ and $w_{\text{in}} = 0$, $T_{\text{in}} = T_\infty$ and $k_{\text{in}} = 3.75\times10^{-5}U_\infty^2$. The inlet dissipation rate is $\varepsilon_{\text{in}} = k_{\text{in}}^{1.5}/(4.46\times10^{-1}D)$. Across the outlet, plane CDdc far from the plate, zero gradients of variables in the stream-wise direction, $\partial()/\partial x = 0$, are imposed. Although this boundary condition is valid for fully developed

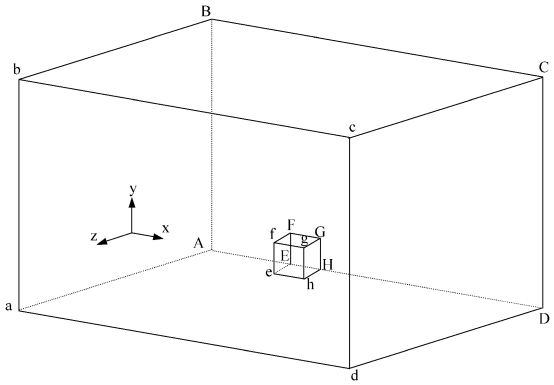

Fig. 3. The computational domain (half section of the cube).

condition, its use in other flow conditions is also permissible for computational convenient provided the outlet boundary is located in a region where the flow is in the downstream direction and sufficiently far from the region of interest. For plane BCcb, a free-stream condition is assumed. Free-stream temperature is assumed 25 °C and the base surface of the blocks, plane HheE, is assumed to be at 75 °C. The block material is taken aluminum with thermal conductivity 202 $\text{W}\cdot\text{m}^{-1}\cdot\text{K}^{-1}$, that is widely used for heat removal fins.

For plane AEFGHDCB, FGHE and abcd, symmetry conditions are assumed, that on these planes zero cross-stream gradient condition, $\partial()/\partial z = 0$, is specified with $w = 0$. The near wall values for the parallel velocity components, temperature, the turbulent kinetic energy and its dissipation rate are determined from the standard log-law based wall function (Launder and Spalding [13]).

4. Computational scheme

4.1. Domain geometry and grid size

The domain used in these calculations consists of an entrance region sufficiently far from the cube surfaces for applying free stream condition, the plane AabB and BCcb, symmetry condition for plane abcd and outlet condition for the plane CDdc as illustrated in Fig. 3. These boundaries should be far enough that the results be independent from the boundary position. Although for plane AabB slight effects of turbulent boundary layer development may affect the results. However, upstream boundary position may be depends on the position of fan, which may contribute to different conditions. The choice of computational domain is based on the previous numerical simulations of the other authors, two and three-dimensional investigations performed for determining upstream and downstream dimensions in "x" direction, approaching the free-stream flow condition in "y" direction, computational time and limitations without losing any accuracy and also monitoring the validity of the results. In the present conditions, several testes were made and finally the computational domain extends $5D$ upstream, $15D$ downstream and $10D$ in y direction and

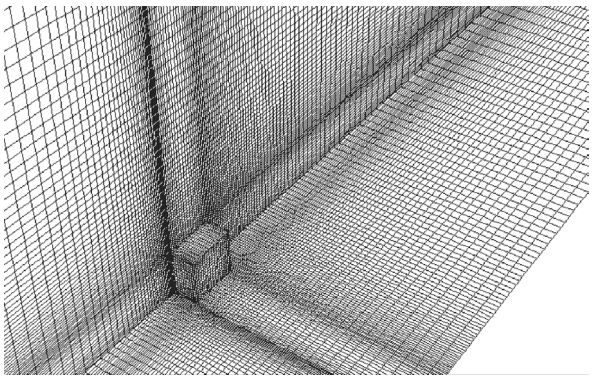

Fig. 4. Typical grid configuration of the computational domain on the cube and the base plate ($Br = 10\%$).

Table 1
Grid independent studies for blockage ratio of $Br = 10\%$

Grid	$\overline{C_f}$	$\overline{Nu}$
$120 \times 50 \times 30$	0.00361	327.46
$135 \times 55 \times 35$	0.00336	348.13
$150 \times 63 \times 40$	0.00317	365.71
$165 \times 70 \times 45$	0.00301	384.34
$180 \times 80 \times 50$	0.00297	389.14

Table 2
The effect of domain region on the flow and heat transfer parameters

Geometry	$\overline{C_f}$	$\overline{Nu}$
Whole domain	0.01372	40.06
Half section domain	0.01415	41.95

from D (for $Br = 50\%$) to $5D$ (for $Br = 10\%$) in z direction.

The next step is an appropriate grid points in the three-dimension. The solution should be independent of grids and for this respect, several grid distributions was studied. For each grid the average friction coefficient and average Nusselt number is determined and typical calculation is presented in Table 1. From these results and also with monitoring and comparing the pressure and velocity values for each grid size, it is found that for an array with $Br = 10\%$, the number of grid points in the x, y and z direction of $165 \times 70 \times 45$, are adequate. The grid configuration for the sample cube is shown in Fig. 4. According to the cubical shape of the block, block's aspect ratio and height ratio are both 1.

To verify the half region effect on the flow parameters and comparing result with the whole region, computation is carried for $Re = 4.2 \times 10^3$, $D/W = 10\%$ and average friction coefficient and average Nusselt number is determined. Table 2 shows that the results are very close to each other. However, the computation time for the whole domain was about 12 hr while for half section it was about 8 hr which has considerable differences.

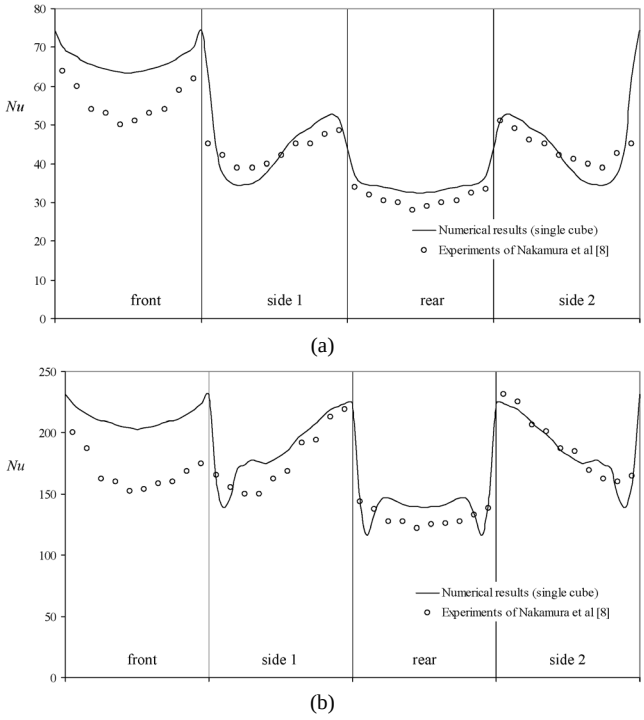

Fig. 5. Comparison of the local Nusselt number at the mid-plane section ($y/D = 0.5$) of a cube at different Reynolds numbers with experimental measurement of Nakamura et al. [8]: (a) $Re = 4.2 \times 10^3$; (b) $Re = 3.3 \times 10^4$.

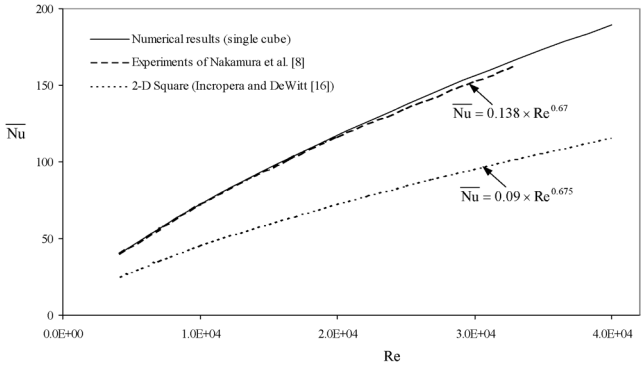

Fig. 6. Comparison of the average overall Nusselt number obtained by numerical simulation with experimental measurements of Nakamura et al. [8].

4.2. Computational procedure

The governing equations of turbulent three-dimensional flow are solved using a *finite volume* discretization code, in which the control volume cells for velocity components are staggered with respect to the main control volume cells [14]. To solve these equations numerically, *Simplec* algorithm [15] is employed. The accuracy of the numerical scheme is validated by comparing the results with experimental studies of Nakamura et al. [8], that it's experimental configuration is very similar to the present computation geometry. Result is presented in Figs. 5 and 6 for the local and overall values of Nusselt number respectively. For this validation, a half section of a cube with $Br = 5\%$ con-

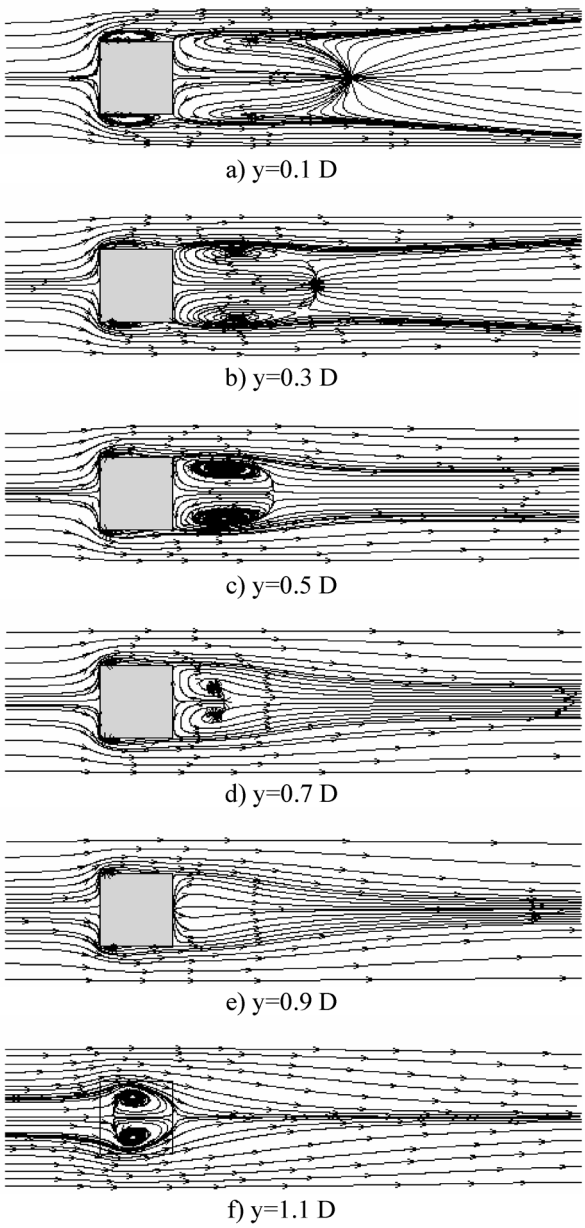

Fig. 7. Typical particle paths around a cube at different height ($Re = 2.5 \times 10^4$ and $Br = 50\%$).

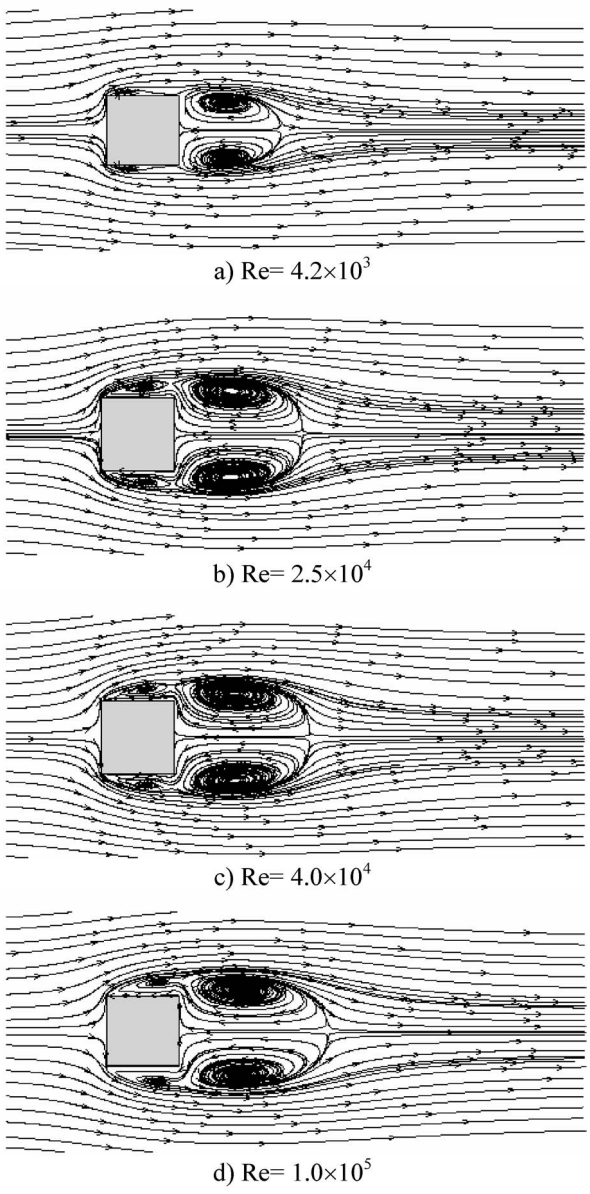

Fig. 8. Typical particle paths around a cube at different Reynolds numbers ($y = 0.5D$ and $Br = 10\%$).

sidered and boundary conditions are similar to those presented in Section 3, except that plane abcd assumed to have free-stream conditions. Local comparison of Nusselt number are presented in Fig. 5(a) and (b) at $y/D = 0.5$ in mid-plane section of a cube at $Re = 4.2 \times 10^3$ and $Re = 3.3 \times 10^4$ respectively and very good agreement is observed by comparing the average results with experimental measurements of Nakamura et al. [8]. The difference over the front surface and the edges may be due to the sharp gradient of flow in the computation relative to the measurements. This figure also shows symmetry of convection on the side surfaces, which verify also the assumption of the selection of the half domain region. Also, Fig. 6 illustrates the comparison of average overall Nusselt number over all the block surfaces which indicates an excellent agreement. In this figure, variation of Nusselt number for a two-dimensional square is also presented which shows strong three-dimensional effects on enhancing convection heat transfer. The differences increase with increasing Reynolds number.

5. Results and discussion

Numerical studies are made for a wide range of Reynolds number of 4.2×10^3 to 1×10^5 (for $Pr = 0.7$) and blockage ratio from 10 to 50% and for each test, calculations was carefully monitored through fluid flow, heat transfer and field variables to determine a stationary state and reliable results.

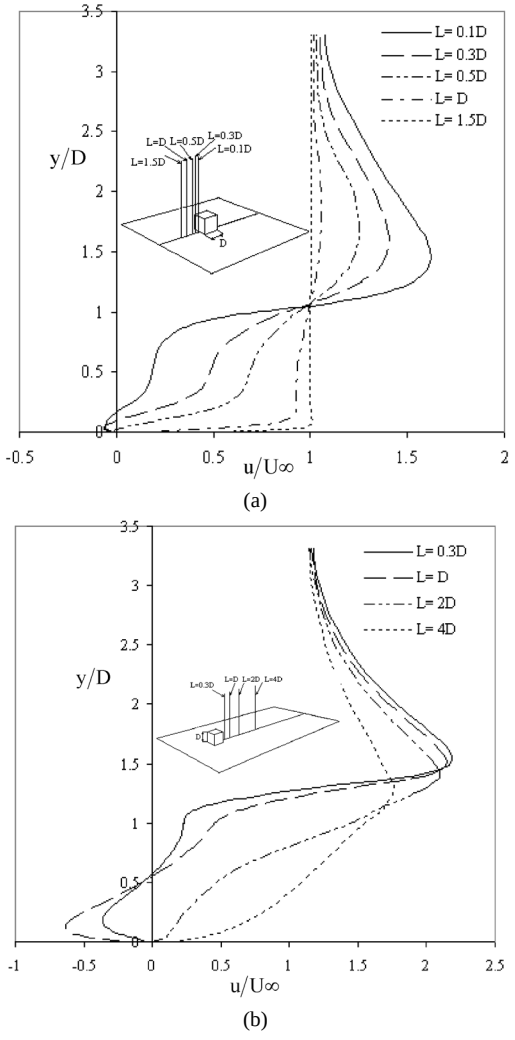

Fig. 9. Typical velocity profiles in the stream-wise direction for various positions ($Re = 2.5 \times 10^4$ and $Br = 30\%$): (a) in front of the cube; (b) behind the cube.

Fluid particle paths around a cube in an array of cubes at different heights are shown in Fig. 7. Over the base plate, a horseshoe vortex is formed in the front of cube and stretches in stream-wise direction. In this case, with increasing blockage ratio, width of bubbles in cross-stream direction reduced but the length of bubbles enlarged.

It is visible that bubbles are not freely formed on the blocks side surfaces because of the small spacing between the cubes. Symmetry condition between the blocks is dominant and corresponding flow is different from a single block with free span wise domain. Form Fig. 7, it can be obtained that the length of recirculating bubble decreases from top surface to the base plate due to the effects of the base plate. Extend of the wake in the leeward side of cube illustrates that recirculation is different at different heights and flow over the cube top surface also have strong recirculations without reattachment [1,2]. Fluid particle paths around a cube for different Reynolds numbers are presented in Fig. 8. Comparing Fig. 8(a) with (d), one can observe that for low Reynolds number ($Re = 4.2 \times 10^3$), the wake size is about

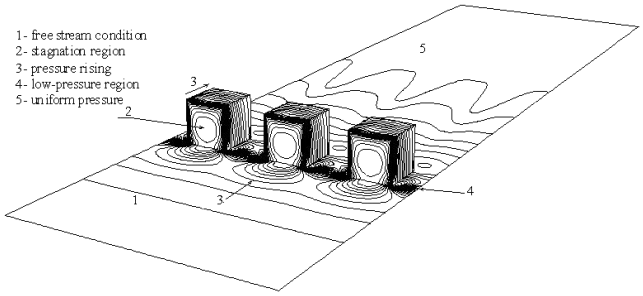

Fig. 10. Typical $3D$ contours of pressure over an array of cubes mounted over a surface ($Re = 2.5 \times 10^4$ and $Br = 50\%$).

the cube dimension (D) but for a higher Reynolds number (for $Re = 10^5$), wake region extends more than $2D$. These figures indicate that the length of arch-shaped bubble that formed behind the cubes becomes larger with increasing Reynolds number and cube disturbance diminish after wider distance. Also with increasing Reynolds number the bubble enlarged widely in the cross-stream direction. However for such a high Reynolds number, there is not any flow reattachment on the block side surfaces.

Comparing Fig. 7(c) with Fig. 8(b), it is visible that bubbles formed over the sides of the cubes with lower blockage ratios have grown freely rather than those for larger blockage ratios. Such boundary layer disrupting will influences the rate of heat transfer from the cubes and causes better cooling.

Variation of velocity profiles in stream-wise direction along various lines in forward and leeward side of the cube is shown in Fig. 9(a) and (b) respectively. In this figure, "L" is the stream-wise distance between the vertical lines and forward face (a) or rear face (b) of the cube. It should be noted that in the recirculating bubbles around the cubes, x-velocity direction is opposite to the upcoming flow direction. However further downstream turbulent boundary layer starts to developing and effects of perturbation diminishes. In the upstream region, closed to the cube, reverse velocity distribution is observed. Also behind the cube, in the recirculating bubble (arch-shaped vortex), negative velocity values is obtained.

Pressure field around the cubes are shown in Fig. 10. This figure shows high values of pressure on the front face of the cubes due to the flow stagnation and low pressure on the backward face. Over the side surfaces and behind the cubes, in the wake, smaller values of pressure observed due to the recirculating bubbles formed over these regions. Far from the cubes, in upward and downward direction, a uniform pressure distribution observed due to the sufficient distance from the cubes boundaries.

Two-dimensional pressure distributions around the cube for the mid-cube section (a) and a plane over the base plate (b) is illustrated in Fig. 11. In these figures, pressure field on the mid-plane section of the cube along the stream-wise direction shows low-pressure area behind the cube as well as over the top surface where the fluid flow has reversing direc-

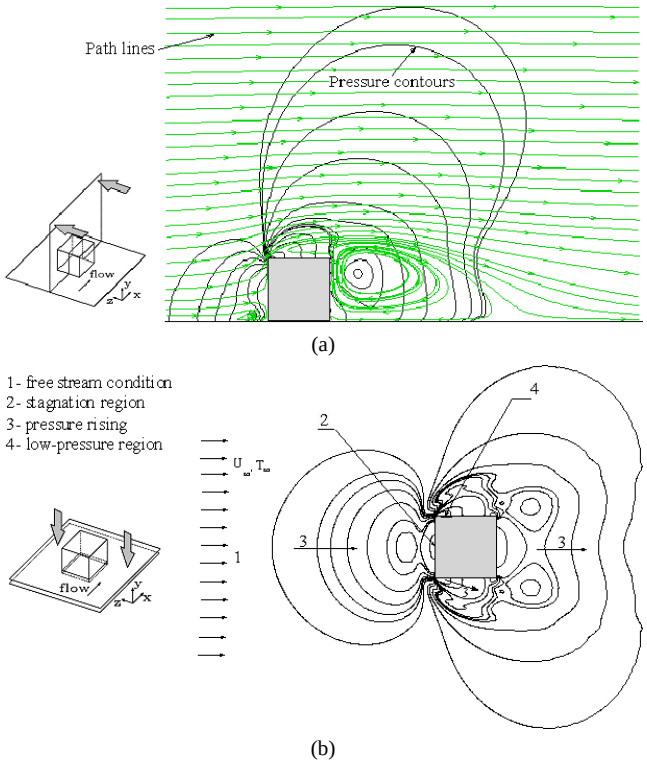

Fig. 11. Typical 2D contours of pressure in two sections of a cube mounted over a surface ($Re = 7.5 \times 10^4$ and $Br = 10\%$).

tion. Fig. 11(b) shows high-pressure region in the stagnation area as marked in the illustration.

Dimensionless drag coefficient may be defined as:

$$C_D = \frac{F_D}{A_c(\frac{1}{2}\rho U_\infty^2)} \tag{5}$$

where F_D is drag force acting on the cube surfaces. This force has two components, one of which is due to the boundary layer surface shear stress (friction drag), the other component is due to a pressure differential in the flow direction resulting from wake formation (form or pressure drag). A_c is the cube frontal area (the area projected perpendicular to the free stream velocity). Variation of the average drag coefficient over the cube side surfaces is presented in Fig. 12. Comparison of the results with correlations presented by Incropera and DeWitt [16] for drag coefficient for two-dimensional circular cylinder in cross flow and for a sphere shows consistent trends. The higher is the blockage ratio, the larger is the value of drag coefficient for the same Reynolds number. This figure also indicates that the results of single cube [10] is nearly the same for the case of blockage ratio of 10%. In this figure results obtained for a single cube by numerical simulation is also added.

Average friction factor coefficient is calculated by:

$$\overline{C_f} = \frac{\bar{\tau}_w}{\frac{1}{2}\rho U_\infty^2} \tag{6}$$

where $\bar{\tau}_w$ is the average wall shear stress over the cube side surfaces. For the studies considered, wall shear stress is determined over the surfaces and its average value is calculated for each condition. Variation of average friction factor coefficient ($\overline{C_f}$) over the cube side surfaces versus Reynolds number is illustrated in Fig. 13. For all cases, the average friction factor coefficient decreases with increasing Reynolds number, which is similar to the flow across two-dimensional circular cylinder. For this case, average friction coefficient over a single cube is also added and it can be concluded that for smallest blockage ratio ($Br = 10\%$), results are in good agreement with the results obtained for a single cube mounted over a surface. This means that blockage ratios less than 10% have no effects on the fluid structure around the cubes.

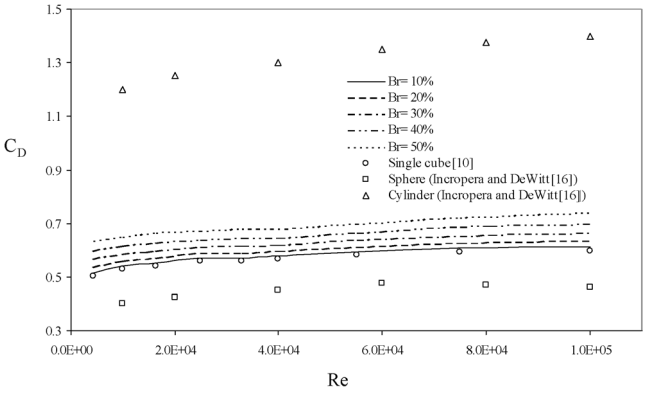

Fig. 12. Comparison of the variation of average drag coefficient over the cube surfaces with other geometries.

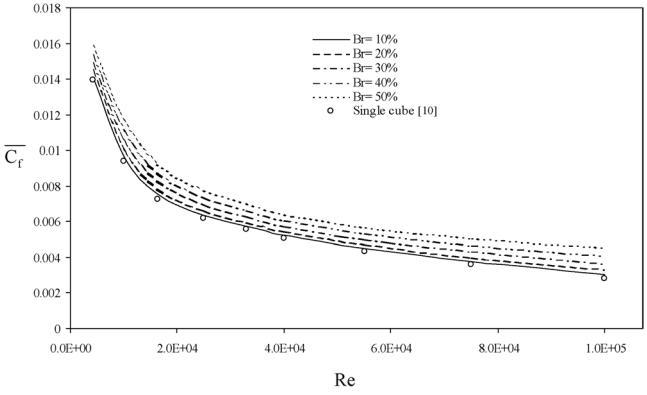

Fig. 13. The variation of average friction coefficient over the cube surfaces for different Reynolds numbers and blockage ratios.

Fig. 14 illustrates the temperature distribution over the cubes side surfaces with 0.5 °C increments. It can be seen that area about one-third of cube's height near the top surface is at constant temperature of about 70 °C. In the region behind the cubes, in the wake, temperature distribution is near the ambient temperature. Temperature differences over the cubes surfaces are very small which is due to high thermal conductivity of cubes. It seems that these cubes are acting as a resistance imposing the upcoming fluid flow and they will have strong effects on the increasing rate of heat transfer from the base plate if one considers them as local surface roughness. Two-dimensional temperature distribu-

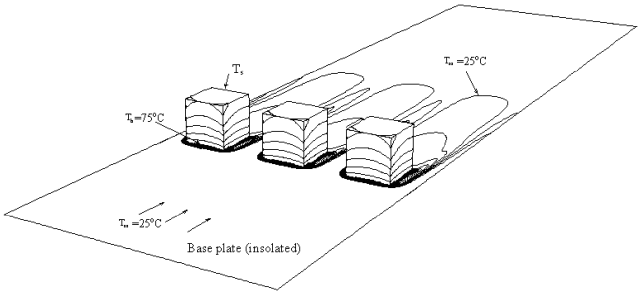

Fig. 14. Typical 3-D contours of cubes surface temperature ($Re = 2.5 \times 10^4$ and $Br = 50\%$, $T_b = 75\,^\circ\mathrm{C}$, $T_\infty = 25\,^\circ\mathrm{C}$, increment $= 0.5\,^\circ\mathrm{C}$).

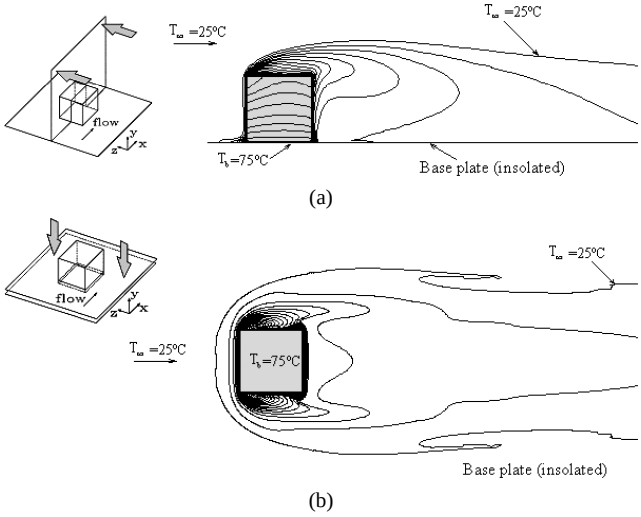

Fig. 15. Typical $2D$ contours of temperature around the cube ($Re = 7.5 \times 10^4$ and $Br = 10\%$, $T_b = 75\,^\circ\mathrm{C}$, $T_\infty = 25\,^\circ\mathrm{C}$, increment $= 0.5\,^\circ\mathrm{C}$).

tions in two different sections of a cube is shown in Fig. 15. In this figure, the values of several temperature contours are marked and large temperature gradients are shown in the front face. This pattern indicates high convective heat transfer, while low temperature gradients in the back face near the base-plate show low convection heat transfer region, similar to the observation of [8,11].

Average overall Nusselt number over a cube surfaces in an array of cubes is obtained from numerical simulation and presented in Fig. 16. Overall convective heat transfer increases with increasing flow Reynolds number and blockage ratio, which is due to the strong effects of flow recirculation on the side surfaces.

For the range of Reynolds numbers of 4.2×10^3 to 1×10^5 and blockage ratios from 10 to 50%, numerical results are combined and a correlation for average Nusselt number developed to include both effect of Reynolds number and blockage ratios when air with $Pr = 0.7$ blows parallel to an array of block as follows:

$$\overline{Nu} = 0.11 Re^{0.702}(1 + 0.68Br) \tag{7}$$

Results show that for a cube in an array, convective coefficient is higher than single block and also from a two-

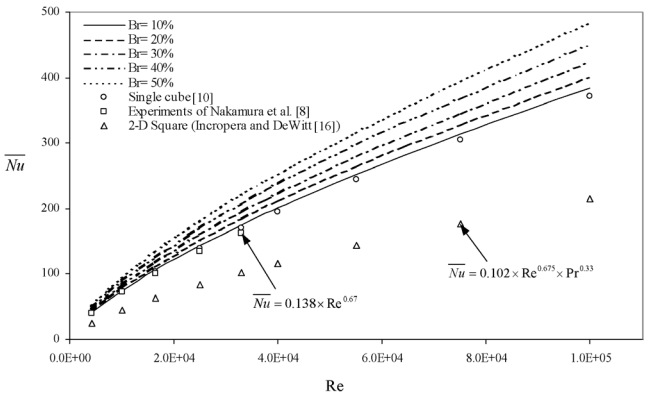

Fig. 16. Comparison of the variation of average Nusselt number over the cube with other studies ($Pr = 0.7$).

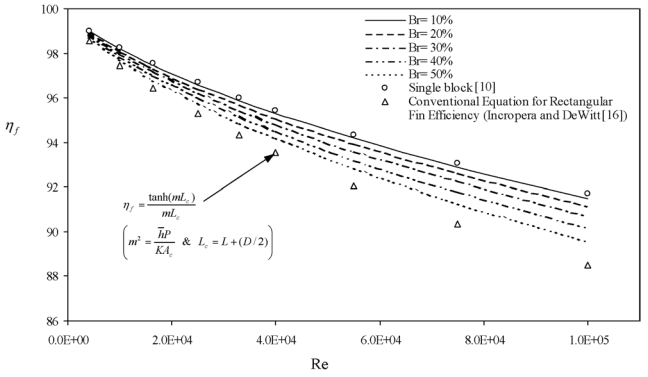

Fig. 17. Variation of the fin efficiency for an array of cubes with different blockage ratios.

dimensional square block in cross-stream flow condition. The correlation (7) fitted with average of 0.79% and maximum 2.17% deviation and shows that convective heat transfer increases linearly with closing the space between blocks.

In the present computations, the cubes can be considered as finite low fins attached over a surface such as in heat exchangers or heating elements. Conjugate conduction and convection heat transfer can simulate the fin performance for various flow and fin spacing. Fin thermal performance can be provided by fin efficiency

$$\eta_f = \frac{q_f}{q_{\max}} = \frac{q_f}{\bar{h} A_f (T_b - T_\infty)} \tag{8}$$

From the computations performed local convection and temperature over the entire surfaces of the cube is calculated and the rate of heat transfer q_f is determined by $q_f = \sum h \Delta A (T_s - T_\infty)$. Variation of the fin efficiency η_f is determined from relation (8) and presented in Fig. 17. It is obvious that fin efficiency for these cubic blocks is high due to the small height of these prisms and less resistance opposing convective heat transfer. Comparison of the results with correlation proposed by Incropera and DeWitt [16] for the rectangular fins shows similar trends but corresponding fin efficiency is higher from three-dimensional fins with adiabatic tips for the same Reynolds number. This result is similar to the observation of Nusselt number in Fig. 16. The

fin efficiency is reduced by increasing flow Reynolds number.

Based on the numerical results, a correlation for fin efficiency obtained, including the effects of Reynolds number and blockage ratio. For the range of Reynolds numbers of 4.2×10^3 to 1×10^5 and blockage ratios from 10 to 50%, the correlation is:

$$\eta_f = 126.69 Re^{-0.027} (1 + Br)^{-0.035} \quad (9)$$

This correlation fitted with maximum of 2.21% and average of 0.7% deviation.

6. Conclusion

Numerical computation is made considering fluid flow and heat transfer from an array of cubes mounted over a surface with free stream flow and developing boundary layer in the upstream region. Calculations are made for a wide range of Reynolds numbers from $4.2 \times 10^3 < Re < 1 \times 10^5$, blockage ratios from 10 to 50% and $Pr = 0.7$, and following conclusions are made:

(1) Bubble formation is strongly depends upon the upcoming flow properties and cubes blockage ratio. With increasing blockage ratio, width of bubbles in cross-stream direction become smaller but the length of bubbles enlarged which is different from a single cube conditions.
(2) Average friction factor coefficient decreases with increasing Reynolds number, which is similar to the flow across two-dimensional circular cylinder. Also average friction factor coefficient increases with increasing blockage ratio.
(3) Overall convective heat transfer increases with increasing flow Reynolds number and blockage ratio. Average convection on the front surface is higher for all Reynolds numbers. However, convective heat transfer is low over the back surface for all Reynolds numbers.
(4) For an array of cubes in cross-stream direction, for the range of Reynolds numbers of 4.2×10^3 to 1×10^5 and blockage ratios from 10 to 50%, a correlation for average Nusselt number is developed as $\overline{Nu} = 0.11 Re^{0.702} \times (1 + 0.68 Br)$.
(5) Considering such cubic element as a heat sink or a low fin, fin efficiency could determined. Results show that, fin efficiency reduced with increasing Reynolds number and cubes blockage ratio. Fin efficiency for these cubic blocks is high due to the small height of these prisms and less resistance opposing convective heat transfer.
(6) Analyzing the combined conduction and convection, a correlation for fin efficiency, including the effects of Reynolds number and blockage ratio is obtained as $\eta_f = 126.69 Re^{-0.027} (1 + Br)^{-0.035}$.

Acknowledgement

This work is carried at High Performance Computer Center of Shiraz University.

References

[1] I.P. Castro, A.G. Robins, The flow around a surface-mounted cube in uniform and turbulent streams, J. Fluid Mech. 79 (2) (1977) 307–335.
[2] H.J. Hussein, R.J. Martinuzzi, Energy balance for the turbulent flow around a surface mounted cube placed in a channel, Phys. Fluids 8 (1996) 764–780.
[3] R.J. Martinuzzi, C. Tropea, The flow around surface mounted prismatic obstacle placed in fully developed channel flow, J. Fluids Engrg. 115 (1993) 85–92.
[4] M. Faghri, Y. Asako, Prediction of turbulent three-dimensional heat transfer of heated blocks using low Reynolds number two-equation model, ASME HTD 206 (1) (1992) 39–45.
[5] E.R. Meinders, K. Hanjalic, Vortex structure and heat transfer in turbulent flow over a wall-mounted matrix of cubes, Internat. J. Heat Fluid Flow 20 (1999) 255–267.
[6] E.R. Meinders, G.M.P. van Kempen, L.J. van Vliet, T.H. van der Meer, Measurement and application of an infrared image restoration filter to improve the accuracy of surface temperature measurements of cubes, Experiments Fluids 26 (1999) 86–96.
[7] E.R. Meinders, T.H. van der Meer, K. Hanjalic, Local convection heat transfer from an array of wall-mounted cubes, Internat. J. Heat Mass Transfer 41 (2) (1998) 335–346.
[8] H. Nakamura, T. Igarashi, T. Tsutsui, Local heat transfer around a wall-mounted cube in the turbulent boundary layer, Internat. J. Heat Mass Transfer 44 (2001) 3385–3395.
[9] B. Niceno, A.D.T. Dronkers, K. Hanjalic, Turbulent heat transfer from a multi-layered wall-mounted cube matrix: A large eddy simulation, Internat. J. Heat Fluid Flow 23 (2002) 173–185.
[10] E. Velayati, M. Yaghoubi, Analysis of conjugate heat transfer around a wall-mounted cube, in: Proceedings of 8th Iranian Fluid Dynamics Conference, September 8–10, University of Tabriz, Tabriz, Iran, 2003.
[11] E. Velayati, M. Yaghoubi, Numerical study of convective heat transfer from an array of parallel bluff plates, Internat. J. Heat Fluid Flow 26 (2005) 80–91.
[12] V. Yakhot, S.A. Orszag, S. Thangam, T.B. Gatski, C.G. Speziale, Development of turbulence models for shear flows by a double expansion technique, Phys. Fluids A 4 (7) (1992) 1510–1520.
[13] B.E. Launder, D.B. Spalding, The numerical computation of turbulent flow, Comput. Methods Appl. Mech. Engrg. 3 (1974) 269–289.
[14] S. Patankar, Numerical Heat Transfer and Fluid Flow, Hemisphere, Washington, DC, 1980.
[15] J.P. Vandoormaal, G.D. Raithby, Enhancements of the simple method for predicting incompressible fluid flows, Numer. Heat Transfer 7 (1984) 147–163.
[16] F.P. Incropera, D.P. DeWitt, Fundamentals of Heat and Mass Transfer, fourth ed., Wiley, New York, 1996.